

# Coherent Three-Photon Excitation of the Strontium Clock Transition

Junyu He (何君钰)<sup>1</sup>, Benjamin Pasquiou<sup>1,2,3,4</sup>, Rodrigo González Escudero<sup>1</sup>,  
Sheng Zhou (周晟)<sup>1</sup>, Mateusz Borkowski<sup>1</sup> and Florian Schreck<sup>1,2,\*</sup>

<sup>1</sup>Van der Waals-Zeeman Institute, Institute of Physics, University of Amsterdam,  
Science Park 904, 1098XH Amsterdam, The Netherlands

<sup>2</sup>QuSoft, Science Park 123, 1098XG Amsterdam, The Netherlands

<sup>3</sup>CNRS, UMR 7538, LPL, F-93430, Villeteuse, France

<sup>4</sup>Laboratoire de Physique des Lasers, Université Sorbonne Paris Nord, F-93430, Villeteuse, France

(Dated: June 24, 2024)

We recently demonstrated a continuous Bose-Einstein condensate of strontium atoms. We could turn this into a continuous-wave atom laser if an efficient outcoupling mechanism is found. Here we show a coherent three-photon excitation of the clock transition in a strontium BEC with contrast of 44.6(3.5)%. We follow it up with a demonstration of three-photon STIRAP-like transfer. Our work constitutes an essential step towards the outcoupling of a continuous atom laser beam and provides a robust excitation mechanism for quantum simulation.

Two-valence-electron atoms like Sr and Yb offer significant advantages over alkali atoms for quantum sensing [1–3] and offer new possibilities for quantum simulation [4, 5] and computing [6, 7]. These advantages originate in a narrow-line transition enabling laser cooling to the microkelvin scale, a ground state free of electronic magnetic moment ( $^1S_0$ ), long-lived optically excited states ( $^3P_{0,2}$ ), single-photon Rydberg transitions from those states, and an ultranarrow optical clock transition ( $^1S_0 - ^3P_0$ ). Among these features, the clock transition provides the frequency reference in the most precise clocks [8], enables elegant atom interferometric gravitational-wave detectors [2, 3], and qubits [6, 9, 10].

Bosonic strontium provides experimental opportunities not offered by the fermionic isotope. Only bosons allow the creation of Bose-Einstein condensates (BECs) and atom lasers, which are indispensable tools for quantum simulation [11] and promising for quantum sensing based on atom interferometry [12, 13]. Driving the clock transition opens important additional possibilities for bosons, such as the construction of simplified clocks, atom interferometric gravitational-wave antennas, or the outcoupling of an atom laser beam from a steady-state BEC [14]. The clock transition can be opened by applying a magnetic field [15–18]. However, this technique only yields small Rabi frequencies unless one uses intolerably high magnetic fields or light intensities. Instead, one could use a three-photon Raman transfer scheme [19, 20] based on a system of four levels: the ground state  $^1S_0$ , clock state  $^3P_0$ , and two intermediate states,  $^3P_1$  and  $^3S_1$  [Fig. 1(a)].

Here we demonstrate a coherent three-photon Raman transfer of Sr atoms on the clock transition. First, using a  $^{84}\text{Sr}$  BEC as a starting point, we observe Rabi oscillations between the ground state  $^1S_0$  and the excited clock state  $^3P_0$ . Second, we use the same scheme to demonstrate Stimulated Raman Adiabatic Passage (STIRAP), overcoming its usual limitation to odd level numbers [21]. Third, in a thermal gas, we measure the two-body loss coefficient for collisions of clock-state atoms.

Throughout this work we either use a pure BEC or a thermal gas of  $^{84}\text{Sr}$ . Briefly, we load atoms from a red Sr magneto-

optical trap (MOT) into a crossed optical dipole trap, extinguish the MOT, and perform evaporative cooling [14, 22]. The dipole trap consists of a horizontally-propagating elliptical reservoir beam with waists  $120\ \mu\text{m}$  horizontally and  $14.5\ \mu\text{m}$  vertically, and a vertically-propagating dimple trap with a beam waist of  $27\ \mu\text{m}$  [Fig. 1(b)]. Both use 1070-nm light. We obtain pure BECs of about  $10^5$  atoms. When a  $\mu\text{K}$ -level thermal gas is needed, we stop evaporation early.

For our three-photon Raman scheme [Fig. 1(a)] it is critical that we maintain excellent coherence between the three lasers driving it. To do so, we first generate the 689-nm light for the  $^1S_0 - ^3P_1$  transition using an injection-locked diode laser, which amplifies light from our MOT laser. The MOT laser has a full width at half-maximum of approximately 1.5 kHz after locking to a piezo cavity. Then, the frequency of this laser is stabilized to better than 0.5 kHz by locking the cavity length to a saturated-absorption spectroscopy signal [23]. Second, we produce the 688-nm beam for the  $^3P_1 - ^3S_1$  transition using a diode laser whose low output power of 2.5 mW is then in-

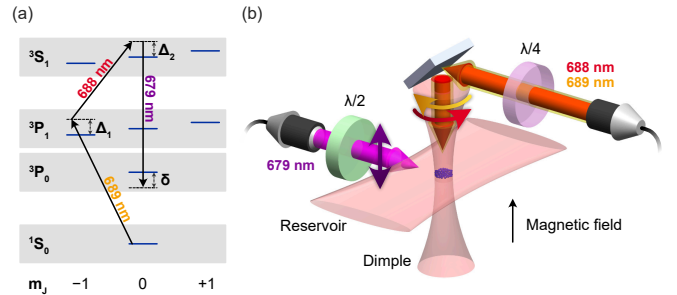


Fig. 1. (a) Levels and transitions relevant for three-photon transfer. We add a non-zero magnetic field to lift the degeneracy between  $m_j$  sub-levels. By controlling the polarizations of the beams, we drive the three-photon transfer through specific sub-levels that avoid destructive interferences between potential transfer paths.  $\Delta_1$ : one-photon detuning for 689-nm.  $\Delta_2 - \Delta_1$ : one-photon detuning for 688-nm.  $\delta$ : three-photon detuning. (b) Geometry of dipole traps and three-photon transfer beams. Colored arrows denote photon polarizations.

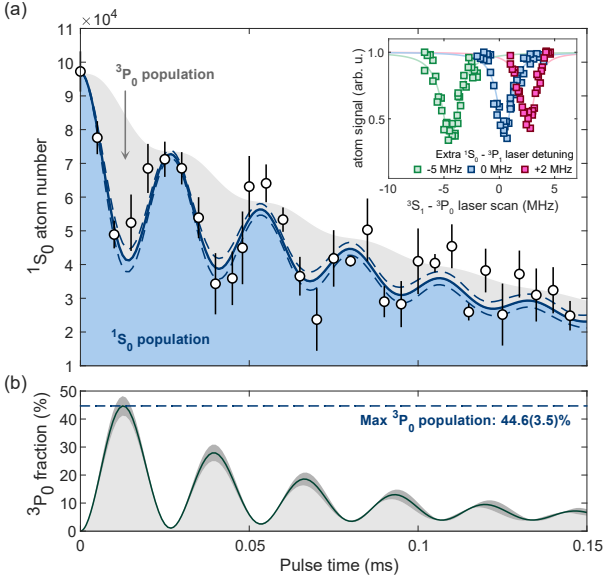


Fig. 2. (a) Coherent three-photon transfer between  $^1S_0$  and  $^3P_0$  state. The experimental data (open black circles) is fitted with a dynamics model using optical Bloch equations [Eq. (1)]. We determine an effective Rabi frequency of  $2\pi \times 37.4(6)$  kHz. Dashed lines denote the error of the fit. Inset: the three-photon line observed by scanning the frequency of the third,  $^3S_1$ - $^3P_0$ , photon. As we change the frequency of the first,  $^1S_0$ - $^3P_1$  photon, we see a corresponding shift in the resonance position. (b) Clock state population according to the fitted optical Bloch equations model. At a pulse length of  $12.5 \mu\text{s}$  we reach a maximum population of  $44.6(3.5)\%$ . Shade represents the uncertainty of the fit.

creased to 13 mW using an injection-locked laser. Third, we generate the 679-nm beam for the downward  $^3S_1$ - $^3P_0$  transition using a diode laser that delivers 1.2 mW of power. We phase-lock the three light sources using a transfer cavity having finesse of over 9000, placed under vacuum on vibration-isolating Viton rods. We stabilize the length of the cavity to the reference 689-nm light using a piezo. We then lock the 688-nm and 679-nm lasers to the transfer cavity using the Pound-Drever-Hall technique. Thus, the three laser fields are locked to better than 15 kHz of each other.

The magnetic sublevels of the two intermediate states complicate our four-level picture and could lead to destructive interference between all the possible excitation pathways. To overcome this, we add a 1.78-G, vertically aligned magnetic field as a quantization axis, and carefully select the polarizations and propagation directions of the three laser beams [Fig. 1(a)]. We combine the 689-nm and 688-nm laser beams with orthogonal polarizations in the same polarization-maintaining fiber and let them propagate parallel to the magnetic field. We focus them to a waist of  $23 \mu\text{m}$  at the atom position. Using a quarter-wave plate we switch to circular polarizations to respectively drive the  $\sigma^-$  and  $\sigma^+$  transitions to  $^3P_1$   $m_J = -1$  and then  $^3S_1$   $m_J = 0$ . The 679-nm beam is vertically-polarized, has a waist of  $47 \mu\text{m}$ , and propagates perpendicular to the magnetic field. It drives the  $\pi$  transition to

the  $^3P_0$   $m_J = 0$  state.

Our choice of laser detunings and intensities is a balancing act between achieving a large effective Rabi frequency, reducing off-resonant scattering, and accommodating the dual function of these laser beams in the experimental scheme. For instance, the 689-nm laser operates with an on-resonant Rabi frequency of  $\Omega_1 = 2\pi \times 0.87$  MHz and at a detuning of  $\Delta_1 = 2\pi \times 40$  MHz, which is significantly larger than the natural linewidth ( $2\pi \times 7.5$  kHz [24]) of this transition. The 688-nm laser also serves as a transparency beam [ $\Delta_2 - \Delta_1 = 2\pi \times 7340$  MHz] and large intensity (Rabi frequency of  $\Omega_2 = 2\pi \times 1583$  MHz). Lastly the 679-nm laser completes the Raman scheme with a detuning of  $2\pi \times 7380$  MHz and an on-resonant Rabi frequency of  $\Omega_3 = 2\pi \times 31.1$  MHz. We work within these constraints so that in the future we could employ this scheme to outcouple a continuous atom laser beam from a steady-state BEC [14].

We first demonstrate a coherent three-photon Rabi oscillation [Figure 2(a)]. After preparing the BEC we apply the three-photon pulse by first turning on the 688-nm laser beam and a few  $\mu\text{s}$  later the 689-nm and 679-nm beams. We measure the remaining  $^1S_0$  atom number by absorption imaging after 24 ms of free-flight expansion. By varying the pulse duration we clearly observe several Rabi oscillations within the first  $150 \mu\text{s}$ .

To describe the dynamics of our three-photon Raman transfer we find it sufficient to use an effective two-state density matrix model similar to Ref. [27]:

$$\begin{aligned} \frac{d}{dt}\rho_{gg} &= \frac{1}{2}i\Omega(\rho_{eg} - \rho_{ge}), \\ \frac{d}{dt}\rho_{ee} &= \frac{1}{2}i\Omega(\rho_{ge} - \rho_{eg}) - \left(\Gamma_e + \frac{1}{2}\beta_{ee}\bar{n}\rho_{ee}\right)\rho_{ee}, \\ \frac{d}{dt}\rho_{ge} &= \frac{1}{2}i\Omega(\rho_{ee} - \rho_{gg}) - \frac{1}{2}\left(\Gamma_e + \frac{1}{2}\beta_{ee}\bar{n}\rho_{ee} + 2i\delta\right)\rho_{ge}, \\ \frac{d}{dt}\rho_{eg} &= \frac{1}{2}i\Omega(\rho_{gg} - \rho_{ee}) - \frac{1}{2}\left(\Gamma_e + \frac{1}{2}\beta_{ee}\bar{n}\rho_{ee} - 2i\delta\right)\rho_{eg} \end{aligned} \quad (1)$$

Here  $\rho_{gg}$  and  $\rho_{ee}$  are the ground- and clock-state atom populations and  $\rho_{ge}$  and  $\rho_{eg}$  are the respective coherences;  $\Omega$  and  $\delta$  are the three-photon (on-resonance) Rabi frequency and detuning. We account for the decoherence due to one- and two-body clock-state atom losses via loss coefficients  $\Gamma_e$  and  $\beta_{ee}$ . Using the least-squares method we determine the Rabi frequency  $\Omega = 2\pi \times 37.4(6)$  kHz and an effective detuning of  $\delta = 2\pi \times 25(1)$  kHz. The fitted one-body loss rate  $\Gamma_e = 2\pi \times 6.2(6)$  kHz serves as a catch-all for all one-body decoherence and loss processes. The two-body loss coefficient  $\beta_{ee} = 4.2(2) \times 10^{-11}$  cm<sup>3</sup>/s is determined experimentally below. The initial average density of ground-state atoms  $\bar{n}(t=0) = 2.78 \times 10^{14}$  cm<sup>-3</sup> assumes a Thomas-Fermi profile. Using our fitted model we can also determine the transfer efficiency as a function of pulse length [Fig. 2(b)]. The maximum is reached with a pulse length of  $12.5 \mu\text{s}$ : as much as  $44.6(3.5)\%$  of the initial  $^1S_0$  population is transferred to the clock state.

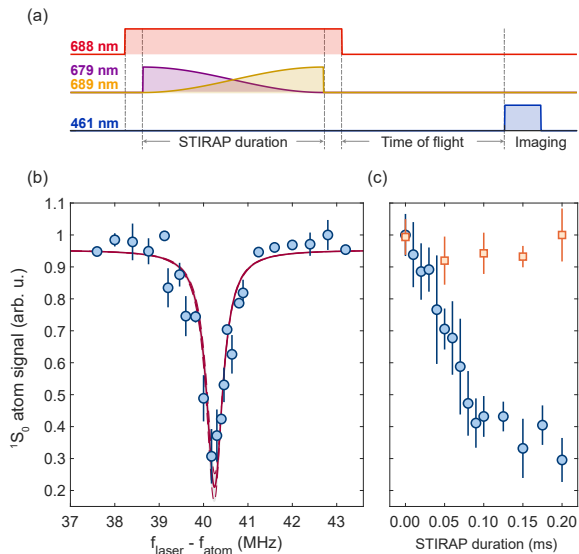


Fig. 3. STIRAP of  $^1S_0$  atoms to the  $^3P_0$  clock state. (a) We execute STIRAP pulses by varying the intensities of the 679-nm and 689-nm lasers, but keeping the 688-nm power constant. We then detect the remaining  $^1S_0$  atom number by time-of-flight imaging. (b) Remaining  $^1S_0$  atom number depending on 689-nm laser detuning for a STIRAP duration of  $150\mu\text{s}$ . Here  $f_{\text{laser}}$  is the frequency of the 689-nm laser and  $f_{\text{atoms}}$  is the frequency of the  $^1S_0 - ^3P_1$  transition at zero magnetic field. (c) Circles: Remaining ground-state atoms as a function of STIRAP pulse duration. Atom loss saturates at about  $150\mu\text{s}$ . Squares: same sequence, but with the 679-nm laser off, showing that all three lasers are needed to perform the transfer.

Next, we demonstrate a STIRAP-like transfer of  $^1S_0$  atoms to  $^3P_0$  [Fig. 3(a)], which provides higher reliability than  $\pi$  pulses. Conventionally STIRAP is perceived to be limited to odd level numbers [21]. Here, we reduce the effective number of states from four to three by coupling the  $^3P_1$  and  $^3S_1$  states using the 688-nm laser operating at constant power. The STIRAP transfer starts by applying 679-nm light but not 689-nm light and then slowly inverting the power ratio between the 679-nm and 689-nm light. A dark eigenstate thus adiabatically evolves from the  $^1S_0$  state into the  $^3P_0$  state. At the end of the transfer, all light is turned off, with the 688-nm one last. With a STIRAP pulse duration of  $150\mu\text{s}$  we obtain a transfer efficiency of up to 74(4)%, based on a Lorentzian fit to  $^1S_0$  loss data [Fig. 3(b)]. Increasing the pulse duration beyond the  $150\mu\text{s}$  does not improve the efficiency [Fig. 3(c)] likely due to two-body losses or off-resonant scattering.

We perform several sanity checks to ensure that we target the  $5s5p\ ^3P_0$  state. We start by testing the resonance condition:

$$f_{689} + f_{688} - f_{679} = f_{^1S_0 \rightarrow ^3P_0}. \quad (2)$$

We vary the frequency of the first photon by several MHz while taking spectra using the third photon frequency [Fig. 2(a), inset]. This results in a corresponding shift of the three-photon line, as expected. Then, we measure the absolute frequencies of the three lasers using a

wavemeter. We obtain the three-photon transition frequency  $f_{^1S_0 \rightarrow ^3P_0} = 429\,227\,720(3)$  MHz, in perfect agreement with the literature  $^{84}\text{Sr}$  clock transition frequency  $f_{^1S_0 \rightarrow ^3P_0} = 429\,227\,716.762(6)$  MHz [28, 29]. Next, we verify that we indeed populate the  $^3P_0$  state. After a  $\pi$ -pulse, we first blow away all  $^1S_0$  atoms. We then recover a signal of  $^1S_0$  atoms by using the 679-nm and 688-nm lasers to two-photon transfer the  $^3P_0$  atoms to the  $^3P_1$  state which then decays to  $^1S_0$ . Next, we verify that the coherent behavior shown in Fig. 2(a) stems from a three-photon, rather than a two-photon transition. In principle the Rabi oscillations could stem from coupling to the bright  $^3S_1$  state and the loss from subsequent decay to the metastable  $^3P_{0,2}$  states. To demonstrate that also the 679-nm laser is crucial, we repeat our STIRAP experiment without turning on that laser. We see no atom loss [squares in Fig. 3(c)]. Last, we compare the fitted Rabi frequency  $\Omega = 2\pi \times 37.4(6)$  kHz to the predictions of a four-level dressed-state model, where

$$\Omega = \left| \frac{\Omega_1 \Omega_2 \Omega_3}{4\Delta_1(\Delta_2 - \Delta_1) - \Omega_2^2} \right| = 2\pi \times 32.2(5.0) \text{ kHz}, \quad (3)$$

assuming a 10% power calibration uncertainty. We find perfect consistency.

Last, we turn our attention to two-body inelastic collisions between clock-state atoms. Clock-state collisions are universally lossy due to molecular formation at short internu-

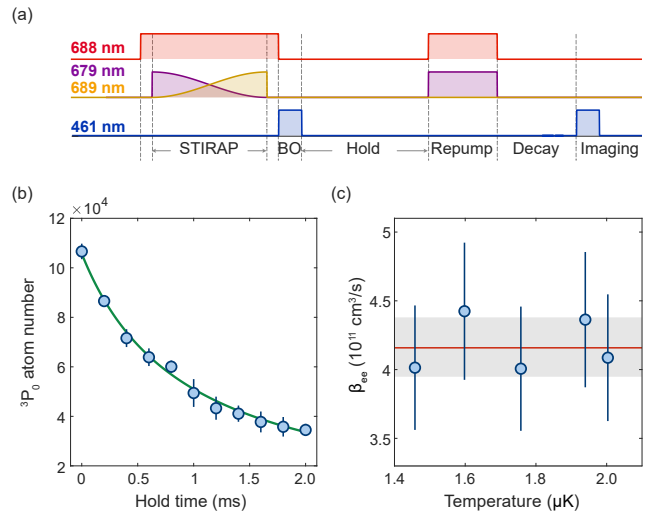


Fig. 4. Measurements of two-body inelastic losses for  $^3P_0$  atoms. (a) We STIRAP-transfer the atoms to the clock state, purge the remaining atoms with a blow-out (BO) pulse and then hold the atoms for collisions to occur. To detect the remaining atoms, we repump them to the  $^3P_1$  state, let them decay to the ground state and then image. (b) Example  $^3P_0$  atom number variation with hold time. The solid green line shows the fit with Eq. (4). The sample temperature is  $1.76\mu\text{K}$ , and the fitted two-body loss coefficient is  $\beta_{ee} = 4.0(5) \times 10^{-11} \text{ cm}^3 \text{ s}^{-1}$ . (c) Two-body collisional loss coefficients  $\beta_{ee}$  for different temperatures. The average across all datasets gives the two-body loss coefficient  $\beta_{ee} = 4.2(2) \times 10^{-11} \text{ cm}^3 \text{ s}^{-1}$  and is shown as a line.

clear separations and have been studied extensively in calcium, strontium and ytterbium [30–38]. The collisional loss rates are typically on the order of  $10^{-11}$  cm<sup>3</sup>/s and prevent the production of clock-state BECs via evaporative cooling.

We measure the two-body loss coefficient of  $^3\text{P}_0$   $^{84}\text{Sr}$  atoms and its dependence on the sample temperature (Fig. 4). To isolate two-body loss from three-body loss we use a dilute thermal sample rather than a BEC. We again start with a STIRAP pulse [Fig. 4(a)], but immediately follow it up with a 15  $\mu\text{s}$ -long blow-out pulse to remove the remaining ground-state atoms from the trap. Then, we hold the atoms in the dark (except for the trapping light) to allow for two-body collisions to occur. Then, we again two-photon transfer, at 37(4)% efficiency, the atoms to the  $^3\text{P}_1$  state and let them decay to the ground state. We then image after a 1.5 ms free-flight expansion. Fig. 4(b) shows the remaining atom number as the hold time is varied; we observe loss on a timescale of  $\sim 2$  ms.

To determine the two-body loss coefficient  $\beta_{ee}$ , we model the time variation of the atom number  $N(t)$  via

$$\frac{dN(t)}{dt} = -\beta_{ee} \frac{n_0}{N_0} N^2(t). \quad (4)$$

The initial density  $n_0 = N_0(\bar{\omega}^2 m/4\pi k_b T)^{3/2}$  assumes a Maxwell-Boltzmann distribution for a temperature  $T$ . The mean trap frequency  $\bar{\omega} = (\omega_x \omega_y \omega_z)^{1/3}$ ; we measured the individual frequencies  $\omega_{x,y,z}$  by observing dipole oscillations of a ground-state thermal gas. We assume that the clock-state atoms inherit the shape of the initial ground-state cloud because the hold time is too short for the atoms to thermalize and adapt to the new trapping potential. We independently measure the temperature of the  $^1\text{S}_0$  cloud before the transfer to the  $^3\text{P}_0$  state via time-of-flight expansion. Even though our model only includes two-body losses, it fully describes the experimental data in Fig. 4(b). Other loss mechanisms can be ignored: trap-induced one-body loss is about  $0.036 \text{ s}^{-1}$ ; three-body losses should also occur at much longer time scales. Our data is insensitive to the latter; we attempted to add them to the model but that failed to improve the quality of the fit.

We measure the two-body loss coefficients for temperatures ranging from 1.4 to 2.0  $\mu\text{K}$  [Fig. 4(c)]. The error bars are dominated by contributions from trap frequency stability,  $^3\text{P}_0$  atom number calibration and to a smaller extent temperature. Within uncertainty, the two-body loss rate is constant in this temperature range, and we obtain an average loss coefficient  $\beta_{ee} = 4.2(2) \times 10^{-11} \text{ cm}^3 \text{ s}^{-1}$ .

Our measured inelastic loss rates can be understood within the universal model [39]. Due to wavefunction symmetry, clock state collisions in  $^{84}\text{Sr}$  can only occur in even partial waves. For our microkelvin sample this is effectively limited to the  $s$ -wave, where the universal model predicts the loss rate coefficient to be independent of temperature. Indeed, our data in Fig. 4(c) shows no thermal variation. We calculate the universal limit,  $\beta_{\text{uni}} = 4h\bar{a}/\mu = 15.7(2) \times 10^{-11} \text{ cm}^3/\text{s}$  using the mean scattering length  $\bar{a} = 2^{-3/2} \frac{\Gamma(3/4)}{\Gamma(5/4)} (2\mu C_6/\hbar^2)^{1/4} = 81.8$  a.u., the van der Waals coefficient  $C_6 = 5360(200)$  a.u. [40], and the reduced mass  $\mu$  equal to half the atomic mass of

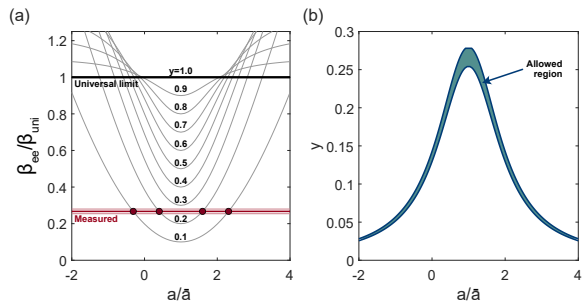


Fig. 5. (a) In the universal model [39], two-body loss coefficients depend on the scattering length  $a$  and a short-range loss probability  $y$ . Our measured loss coefficient  $\beta_{ee} = 4.2(2) \times 10^{-11} \text{ cm}^3/\text{s}$  is four times smaller than the universal limit  $\beta_{\text{uni}}$ . (b) Set of reduced scattering lengths  $a$  and short range loss probabilities  $y$  consistent with the measured loss coefficient shown in panel (a).

strontium. This value is four times larger than our  $\beta_{ee} = 4.2(2) \times 10^{-11} \text{ cm}^3/\text{s}$ . The universal model describes the two-body loss coefficient via the (here unknown) scattering length  $a$  and the short-range loss probability  $y$  [Fig. 5(a)]. Here, having only one measured quantity, we cannot independently determine both  $a$  and  $y$ . For any scattering length  $a$ , there is a matching short range loss probability  $y$  that matches the measured  $\beta_{ee}$  [Fig. 5(b)]. However, we notice that  $y$  reaches a maximum when the scattering length  $a$  equals  $\bar{a}$ , which allows us to determine an upper limit on  $y$ . We conclude that clock-state  $^{84}\text{Sr}$  collisions are not universal with  $y < 0.268(13)$ .

In conclusion, we have demonstrated a coherent transfer of bosonic Sr atoms between ground and excited clock states, starting with a BEC. We have reached a Rabi frequency of 37.4(6) kHz, a transfer efficiency of 44.6(3.5)% and a coherence time that is five times the Rabi oscillation period. Further, we have shown our three-photon scheme allows a STIRAP-like [21] transfer of up to 74(4)% efficiency, as determined from a loss feature. Finally, we measured the two-body loss coefficient for  $s$ -wave collisions of clock-state  $^{84}\text{Sr}$  atoms.

In the future, our scheme could be used to outcouple a cw atom laser beam from a continuously replenished BEC [14]. So far, such a BEC only exists in Sr, where the outcoupling cannot be done by conventional means [12]: Sr is nonmagnetic, so radiofrequency transitions cannot be used; it is also held in a deep dipole trap, so spilling is not an option either. One could use our scheme to coherently transfer atoms to a state for which the dipole trap can easily be engineered to be non-trapping. This would result in a free-falling atom laser beam. Upon excitation, the atoms receive a small net momentum; this can be used to regulate the momentum transfer from null [19, 41] up to the sum of the three photon momenta. On the one hand, a large momentum kick helps outcouple a well-collimated atom laser beam [42]. On the other hand, suppressing the momentum transfer would help create a metastable-state BEC useful for quantum simulation [19]. In a quantum computing context, our technique could push clock qubit gate times to under a microsecond [6].

We are grateful to Z. Idziaszek, P. Thekkepatt, R. Spreew and Z. Guo for helpful discussions. We thank the RbSr team for lending the laser head and N. Grenier for building the 679-nm laser source. This work was supported by the Dutch National Growth Fund (NGF), as part of the Quantum Delta NL programme.

*Author contributions*—J.H. led the experimental effort, with support from R.G.E. and S.Z., performed the data analysis and wrote the manuscript. M.B. contributed the theoretical analysis and cowrote the paper. B.P. conceived the use of the 3-photon Raman scheme as an atom laser outcoupler. J.H., B.P. and F.S. guided the effort. J.H., B.P., M.B. and F.S. discussed the results and F.S. acquired the funding.

*Note*— During the completion of this work, we became aware of concurrent work on the three-photon transition in  $^{88}\text{Sr}$  [43].

---

\* [threePhotonTransfer@strontiumBEC.com](mailto:threePhotonTransfer@strontiumBEC.com)

- [1] A. D. Ludlow, M. M. Boyd, J. Ye, E. Peik, and P. O. Schmidt, Optical atomic clocks, *Rev. Mod. Phys.* **87**, 637 (2015).
- [2] N. Yu and M. Tinto, Gravitational wave detection with single-laser atom interferometers, *Gen. Relativ. Gravit.* **43**, 1943 (2011).
- [3] P. W. Graham, J. M. Hogan, M. A. Kasevich, and S. Rajendran, New Method for Gravitational Wave Detection with Atomic Sensors, *Phys. Rev. Lett.* **110**, 171102 (2013).
- [4] A. V. Gorshkov, M. Hermele, V. Gurarie, C. Xu, P. S. Julienne, J. Ye, P. Zoller, E. Demler, M. D. Lukin, and A. M. Rey, Two-orbital  $SU(N)$  magnetism with ultracold alkaline-earth atoms, *Nature Physics* **6**, 289 (2010).
- [5] F. Gerbier and J. Dalibard, Gauge fields for ultracold atoms in optical superlattices, *New J. Phys.* **12**, 033007 (2010).
- [6] M. Morgado and S. Whitlock, Quantum simulation and computing with Rydberg-interacting qubits, *AVS Quantum Science* **3**, 023501 (2021).
- [7] A. J. Daley, M. M. Boyd, J. Ye, and P. Zoller, Quantum Computing with Alkaline-Earth-Metal Atoms, *Phys. Rev. Lett.* **101**, 170504 (2008).
- [8] A. Aeppli, K. Kim, W. Warfield, M. S. Safronova, and J. Ye, A clock with  $8 \times 10^{-19}$  systematic uncertainty (2024), [arXiv:2403.10664 \[physics.atom-ph\]](https://arxiv.org/abs/2403.10664).
- [9] S. Pucher, V. Klüsener, F. Spriestersbach, J. Geiger, A. Schindewolf, I. Bloch, and S. Blatt, Fine-structure qubit encoded in metastable strontium trapped in an optical lattice, *Phys. Rev. Lett.* **132**, 150605 (2024).
- [10] G. Unnikrishnan, P. Ilzhöfer, A. Scholz, C. Hölzl, A. Götzelmann, R. K. Gupta, J. Zhao, J. Krauter, S. Weber, N. Makki, H. P. Büchler, T. Pfau, and F. Meinert, Coherent control of the fine-structure qubit in a single alkaline-earth atom, *Phys. Rev. Lett.* **132**, 150606 (2024).
- [11] I. Bloch, J. Dalibard, and S. Nascimbène, Quantum simulations with ultracold quantum gases, *Nat. Phys.* **8**, 267 (2012).
- [12] N. P. Robins, P. A. Altin, J. E. Debs, and J. D. Close, Atom lasers: Production, properties and prospects for precision inertial measurement, *Physics Reports* **529**, 265 (2013).
- [13] I. Alonso *et al.*, Cold atoms in space: community workshop summary and proposed road-map, *EPJ Quantum Technology* **9**, 30 (2022).
- [14] C.-C. Chen, R. González Escudero, J. Minář, B. Pasquiou, S. Bennetts, and F. Schreck, Continuous Bose–Einstein condensation, *Nature* **606**, 683 (2022).
- [15] Z. W. Barber, C. W. Hoyt, C. W. Oates, L. Hollberg, A. V. Taichenachev, and V. I. Yudin, Direct excitation of the forbidden clock transition in neutral  $^{174}\text{Yb}$  atoms confined to an optical lattice, *Phys. Rev. Lett.* **96**, 083002 (2006).
- [16] A. Taichenachev, V. Yudin, C. Oates, C. Hoyt, Z. Barber, and L. Hollberg, Magnetic Field-Induced Spectroscopy of Forbidden Optical Transitions with Application to Lattice-Based Optical Atomic Clocks, *Phys. Rev. Lett.* **96**, 083001 (2006).
- [17] T. Akatsuka, M. Takamoto, and H. Katori, Optical lattice clocks with non-interacting bosons and fermions, *Nat. Phys.* **4**, 954 (2008).
- [18] S. Origlia, M. S. Pramod, S. Schiller, Y. Singh, K. Bongs, R. Schwarz, A. Al-Masoudi, S. Dörscher, S. Herbers, S. Häfner, U. Sterr, and C. Lisdat, Towards an optical clock for space: Compact, high-performance optical lattice clock based on bosonic atoms, *Physical Review A* **98**, 053443 (2018).
- [19] D. S. Barker, N. C. Pienti, B. J. Reschovsky, and G. K. Campbell, Three-photon process for producing a degenerate gas of metastable alkaline-earth-metal atoms, *Phys. Rev. A* **93**, 053417 (2016).
- [20] T. Hong, C. Cramer, W. Nagourney, and E. N. Fortson, Optical Clocks Based on Ultranarrow Three-Photon Resonances in Alkaline Earth Atoms, *Phys. Rev. Lett.* **94**, 050801 (2005).
- [21] N. V. Vitanov, A. A. Rangelov, B. W. Shore, and K. Bergmann, Stimulated raman adiabatic passage in physics, chemistry, and beyond, *Rev. Mod. Phys.* **89**, 015006 (2017).
- [22] S. Bennetts, C.-C. Chen, B. Pasquiou, and F. Schreck, Steady-State Magneto-Optical Trap with 100-Fold Improved Phase-Space Density, *Phys. Rev. Lett.* **119**, 223202 (2017).
- [23] S. Stellmer, F. Schreck, and T. C. Killian, Degenerate quantum gases of strontium, in *Annual Review of Cold Atoms and Molecules*, Vol. 2 (World Scientific, 2014) pp. 1–80.
- [24] M. Borkowski, P. Morzyński, R. Ciuryło, P. S. Julienne, M. Yan, B. J. DeSalvo, and T. C. Killian, Mass scaling and nonadiabatic effects in photoassociation spectroscopy of ultracold strontium atoms, *Phys. Rev. A* **90**, 032713 (2014).
- [25] S. Stellmer, B. Pasquiou, R. Grimm, and F. Schreck, Laser cooling to quantum degeneracy, *Phys. Rev. Lett.* **110**, 263003 (2013).
- [26] L. Sonderhouse, C. Sanner, R. B. Hutson, A. Goban, T. Bilitewski, L. Yan, W. R. Milner, A. M. Rey, and J. Ye, Thermodynamics of a deeply degenerate  $SU(N)$ -symmetric fermi gas, *Nature Physics* **16**, 1216 (2020).
- [27] H. J. Metcalf and P. Van der Straten, *Laser cooling and trapping* (Springer Science & Business Media, 1999).
- [28] P. Morzyński, M. Bober, D. Bartoszek-Bober, J. Nawrocki, P. Krehlik, Ł. Śliwczyński, M. Lipiński, P. Masłowski, A. Cygan, P. Dunst, *et al.*, Absolute measurement of the  $^1S_0$ - $^3P_0$  clock transition in neutral  $^{88}\text{Sr}$  over the 330 km-long stabilized fibre optic link, *Scientific Reports* **5**, 17495 (2015).
- [29] H. Miyake, N. C. Pienti, P. K. Elgee, A. Sitaram, and G. K. Campbell, Isotope-shift spectroscopy of the  $^1S_0 \rightarrow ^3P_1$  and  $^1S_0 \rightarrow ^3P_0$  transitions in strontium, *Phys. Rev. Res.* **1**, 033113 (2019).
- [30] M. Bishof, M. J. Martin, M. D. Swallows, C. Benko, Y. Lin, G. Quémener, A. M. Rey, and J. Ye, Inelastic collisions and density-dependent excitation suppression in a  $^{87}\text{Sr}$  optical lattice clock, *Phys. Rev. A* **84**, 052716 (2011).
- [31] R. Bouganne, M. B. Aguilera, A. Dareau, E. Soave, J. Beugnon, and F. Gerbier, Clock spectroscopy of interacting bosons in deep optical lattices, *New J. Phys.* **19**, 113006 (2017).

- [32] L. Franchi, L. F. Livi, G. Cappellini, G. Binella, M. Inguscio, J. Catani, and L. Fallani, State-dependent interactions in ultracold  $^{174}\text{Yb}$  probed by optical clock spectroscopy, *New J. Phys.* **19**, 103037 (2017).
- [33] P. Halder, H. Winter, and A. Hemmerich, Inelastic collisions of optically trapped metastable calcium atoms, *Phys. Rev. A* **88**, 063639 (2013).
- [34] C. Lisdat, J. S. R. V. Winfred, T. Middelmann, F. Riehle, and U. Sterr, Collisional Losses, Decoherence, and Frequency Shifts in Optical Lattice Clocks with Bosons, *Phys. Rev. Lett.* **103**, 090801 (2009).
- [35] A. D. Ludlow, N. D. Lemke, J. A. Sherman, C. W. Oates, G. Quéméner, J. Von Stecher, and A. M. Rey, Cold-collision-shift cancellation and inelastic scattering in a Yb optical lattice clock, *Phys. Rev. A* **84**, 052724 (2011).
- [36] F. Schäfer, H. Konishi, A. Bouscal, T. Yagami, and Y. Takahashi, Spin dependent inelastic collisions between metastable state two-electron atoms and ground state alkali-atoms, *New J. Phys.* **19**, 103039 (2017).
- [37] T. Tomita, S. Nakajima, Y. Takasu, and Y. Takahashi, Dissipative Bose-Hubbard system with intrinsic two-body loss, *Phys. Rev. A* **99**, 031601 (2019).
- [38] A. Traverso, R. Chakraborty, Y. N. Martinez De Escobar, P. G. Mickelson, S. B. Nagel, M. Yan, and T. C. Killian, Inelastic and elastic collision rates for triplet states of ultracold strontium, *Phys. Rev. A* **79**, 060702 (2009).
- [39] Z. Idziaszek and P. S. Julienne, Universal rate constants for reactive collisions of ultracold molecules, *Phys. Rev. Lett.* **104**, 113202 (2010).
- [40] X. Zhang, M. Bishof, S. L. Bromley, C. V. Kraus, M. S. Safronova, P. Zoller, A. M. Rey, and J. Ye, Spectroscopic observation of  $SU(N)$ -symmetric interactions in Sr orbital magnetism, *Science* **345**, 1467 (2014).
- [41] I. I. Ryabtsev, I. I. Beterov, D. B. Tretyakov, V. M. Entin, and E. A. Yakshina, Doppler- and recoil-free laser excitation of Rydberg states via three-photon transitions, *Phys. Rev. A* **84**, 053409 (2011).
- [42] N. P. Robins, C. Figl, S. A. Haine, A. K. Morrison, M. Jeppesen, J. J. Hope, and J. D. Close, Achieving Peak Brightness in an Atom Laser, *Phys. Rev. Lett.* **96**, 140403 (2006).
- [43] S. P. Carman, J. Rudolph, B. E. Garber, M. J. V. de Graaff, H. Swan, Y. Jiang, M. Nantel, M. Abe, R. L. Barcklay, and J. M. Hogan, Collinear three-photon excitation of a strongly forbidden optical clock transition (2024), [arXiv:2406.07902](https://arxiv.org/abs/2406.07902) [physics.atom-ph].